Scientific Reports

https://doi.org/10.1038/s41598-026-44445-0

Article in Press

Integrated machine learning and multi-omics analysis identifies ALOX5 as a potential therapeutic target for tubulointerstitial inflammation in diabetic kidney disease

Received: 1 January 2026

Accepted: 11 March 2026

Published online: 19 March 2026

Cite this article as: Lu W., Deng Y., Zhai L. *et al.* Integrated machine learning and multi-omics analysis identifies ALOX5 as a potential therapeutic target for tubulointerstitial inflammation in diabetic kidney disease. *Sci Rep* (2026). https://doi.org/10.1038/s41598-026-44445-0

Wei Lu, Yiyao Deng, Likang Zhai, Yongqiang Zhang, Die Yang, Kunming Yang, Xue Lu, Ju Zhang, Qiuling Xue, Lunju Luo, Mingming Liu, Hongyan Ren, Xin Xu, Dengmei Ao, Lu Liu, Fangfang Yu, Yuan Ma, Yan Zha & Jing Yuan

Integrated machine learning and multi-omics analysis identifies ALOX5 as a potential therapeutic target for tubulointerstitial inflammation in diabetic kidney disease

Wei Lu[1,+], Yiyao Deng[2,+], Likang Zhai[1], Yongqiang Zhang[3], Die Yang[1], Kunming Yang[1], Xue Lu[3], Ju Zhang[1], Qiuling Xue[3], Lunju Luo[3], Mingming Liu[1], Hongyan Ren[1], Xin Xu[1], Dengmei Ao[4], Lu Liu[2], Fangfang Yu[2], Yuan Ma[1], Yan Zha[2,*], and Jing Yuan[2,*]

[1]Guizhou University, Medical School, Guiyang, 550025, China
[2]Guizhou Provincial People's Hospital, Department of Nephrology, Guiyang, 550002, China
[3]Guizhou University of Traditional Chinese Medicine, the First School of Clinical Medicine, Guiyang, 550005, China
[4]Guizhou Medical University,Clinical Medical College, 550005, China
[*]Correspondence and requests for materials should be addressed to Y.Z. (email: zhayan72@126.com) or J.Y. (email: yuanjinger@126.com)
[+]these authors contributed equally to this work

ABSTRACT

Diabetic kidney disease (DKD) is a leading cause of renal failure. Inflammation of the renal tubules and interstitium is a critical factor in the progression of DKD; however, the key regulatory genes and characteristics of the immune microenvironment remain poorly understood. This study aims to identify key inflammatory biomarkers in the renal tubule tissues of DKD patients and to elucidate their potential immunoregulatory mechanisms. By integrating multiple GEO transcriptome datasets and employing differential expression analysis, weighted gene co-expression network analysis (WGCNA), and machine learning algorithms (LASSO, Random Forest), we identified arachidonate 5-lipoxygenase (ALOX5) as a crucial feature gene of renal tubular inflammation in DKD. Clinical correlation analysis revealed that ALOX5 is significantly upregulated in DKD tissues, with high expression closely associated with decreased glomerular filtration rate and infiltration of M1 macrophages. Additionally, combining single-cell sequencing pseudotime analysis and multiplex immunohistochemistry (mIHC), we demonstrated that ALOX5 and its partner protein ALOX5AP are primarily expressed in $CD68^{+}$ macrophages infiltrating the renal interstitium. They exhibit a high degree of co-localization with NF-κB/p65, iNOS, and CYSLTR1, suggesting that they may mediate the pro-inflammatory polarization of macrophages through the leukotriene-NF-κB axis. Finally, based on molecular docking and ADMET analysis, we screened the natural small molecule honokiol as a potential inhibitor of ALOX5, which possesses favorable pharmacokinetic properties. This study suggests that ALOX5 is a potential biomarker of immune microenvironment imbalance in DKD and provides a rationale for further investigation of targeted anti-inflammatory strategies, with honokiol as a candidate compound.

Introduction

Diabetic kidney disease (DKD) is a leading cause of end-stage kidney disease (ESKD) worldwide[1]. The global burden of DKD is continuously increasing. According to the latest data from the International Diabetes Federation (IDF) in the 11th edition of the "Diabetes Atlas," the total number of adult diabetes patients worldwide is approximately 589 million in 2024, and this is expected to rise to 853 million by 2050. Studies have shown that around 40% of diabetes patients may progress to DKD[2]. In China, the mortality rate across all age groups due to diabetes-related chronic kidney disease has risen from 4.5 per 100,000 people in 1990 to 6.0 per 100,000 in 2016, an increase of 33.3%, indicating a sustained rise in the burden associated with DKD[3]. Although current standard treatments (such as RAS inhibitors) have somewhat delayed the progression of DKD by controlling blood glucose and blood pressure, a significant proportion of patients still eventually progress to ESKD[4]. This is largely due to our inadequate understanding of the pathophysiological mechanisms underlying DKD. Traditional views posit that the pathogenesis of DKD mainly stems from hyperglycemia leading to glomerular hyperfiltration and hemodynamic alterations, which in turn induce the expression of pro-inflammatory and pro-fibrotic factors, resulting in structural and functional damage to the glomeruli and renal tubules through inflammation and fibrosis pathways[5]. However, increasing clinical pathological and experimental evidence suggests that the degree of inflammation and fibrosis in the renal

tubules and interstitium correlates more closely with the decline in renal function than isolated glomerular lesions, indicating that tubular inflammation plays a crucial role in the progression of DKD[6,7]. Tubular inflammation involves epithelial cell injury, inflammatory cell infiltration (macrophages and T cells), oxidative stress, mitochondrial dysfunction, NLRP3 inflammasome activation, and NF-κB activation[8,9]. Despite these findings, key regulatory genes and pathways involved in tubular inflammation remain unclear. In light of these issues, this study aims to systematically identify key inflammatory genes in the renal tubular tissues of DKD and explore their roles within the immune microenvironment. We first integrated multiple GEO datasets and utilized weighted gene co-expression network analysis (WGCNA) and machine learning algorithms to select the important molecule ALOX5, which reflects renal tubular interstitial inflammation. We then verified its potential as a biomarker through clinical correlation analysis. To further elucidate the mechanisms, we employed single-cell sequencing data and multiplex immunohistochemistry (mIHC) techniques to investigate the cellular localization and activation state of ALOX5 and its partner proteins within the renal immune microenvironment. Finally, we predicted potential therapeutic small molecules targeting this pathway using molecular docking techniques and SwissADME. This study not only provides new candidate biomarkers for the treatment of DKD but also offers new theoretical bases for treating DKD through intervention of inflammatory pathways.

Results

Identification of inflammatory genes in DKD

The overall workflow of this study is illustrated in Figure 1. To identify transcriptional alterations in the renal tubular tissues of patients with diabetic kidney disease (DKD), we integrated two datasets: GSE30529 (12 normal samples and 9 DKD samples) and GSE104954 (18 normal samples and 7 DKD samples) as the discovery cohort, which included a total of 30 normal renal tubular samples and 16 DKD renal tubular samples. Two independent datasets, GSE47184 (4 normal samples and 11 DKD samples) and GSE99325 (7 normal samples and 18 DKD samples), were utilized as external validation cohorts. Detailed analytical procedures are described in the "Methods" section and supplementary materials.

Based on the criteria of $|log2FC| > 1$ and a corrected P-value < 0.05, the differential expression analysis conducted in the discovery cohort identified 306 differentially expressed genes (DEGs) between diabetic kidney disease (DKD) and control renal tubular samples, including 205 upregulated genes and 101 downregulated genes. These DEGs were visualized using a volcano plot (Fig 2A; Supplementary Table 4). To further identify gene modules associated with diabetic kidney disease, we performed weighted gene co-expression network analysis (WGCNA). After selecting a soft threshold power (β) of 10, hierarchical clustering and dynamic tree cutting were carried out (Fig 2B). The turquoise module exhibited the strongest positive correlation with the DKD state ($r = 0.77$, $P = 2 \times 10^{-}10$) and comprised 730 genes (Fig 2C-D; Supplementary Table 5). By conducting an intersection analysis among the 306 differential expression genes, the 730 genes from the turquoise module, and 402 inflammation-related genes obtained from the GeneCards database, we identified 37 inflammation-related differentially expressed genes (DEG-IRGs; Supplementary Table 6). Among these, 36 genes were upregulated and 1 gene was downregulated in the context of diabetic kidney disease (Fig 2F). Although the WGCNA filtering step removed only a small number of genes from the DEG/GeneCards overlap, this high concordance suggests that the inflammation-related DEGs were largely concentrated within the DKD-associated turquoise co-expression module.

Functional enrichment analysis of DEG-IRGs

To explore the biological functions of the 37 identified DEG-IRGs, we conducted Gene Ontology (GO) and Kyoto Encyclopedia of Genes and Genomes (KEGG) enrichment analyses. The GO biological process (BP) analysis revealed that these genes were significantly enriched in the positive regulation of leukocyte cell-cell adhesion and leukocyte adhesion (Fig 2G). In the cellular component (CC) category, the genes were primarily enriched in major histocompatibility complex (MHC) protein complexes, secretory granule lumen, and cytoplasmic vesicle lumen (Fig 2I). The GO molecular function (MF) analysis indicated enrichment in peptide antigen binding, MHC class II protein complex binding, and MHC class II receptor activity (Fig 2H). The KEGG pathway analysis showed that the DEG-IRGs were enriched in cellular adhesion molecules (CAMs), type 1 diabetes, and other immune-related pathways (Fig 2J).

Immune cell infiltration and correlations with key immune-related genes

GO and KEGG functional enrichment analyses indicated that the differentially expressed genes were primarily enriched in immune response-related pathways. Based on this, we further utilized the xCell algorithm to infer the abundance of immune cells in DKD versus healthy control renal tissues. The results showed that the overall immune cell composition was altered in DKD (Fig 3A). Specifically, we found that various innate and adaptive immune cells were significantly enriched in DKD tissues, including dendritic cells (DC), monocytes, Th2 cells, CD4+ memory T cells, CD8+ central memory T cells, CD4+ effector memory T cells, mast cells, memory B cells, and plasma cells. In contrast, Th1 cells, regulatory T cells (Treg), and natural killer T (NKT) cells were significantly reduced (Fig 3B). To further investigate the potential synergistic or antagonistic relationships among immune cells within the DKD microenvironment, we constructed a correlation heatmap of the differentially expressed

immune cells (Fig 3C). The results revealed significant positive correlations among inflammation-amplifying cell populations (such as dendritic cells, monocytes, Th2 cells, plasma cells, etc.), suggesting that these cells may form a pro-inflammatory synergistic network in DKD. Conversely, NK and Th1 cells exhibited significant negative correlations with the aforementioned pathogenic cell populations, further confirming the imbalance of immune homeostasis in the DKD microenvironment.

Identification of candidate biomarkers by machine learning

To identify molecular stratification biomarkers for diabetic kidney disease (DKD), we employed two machine learning methods—LASSO regression and random forest—based on the 37 differentially expressed inflammation-related genes (DEG-IRGs). In the LASSO analysis, ten-fold cross-validation was used to determine the optimal penalty parameter. As shown in Fig 3D, at $\lambda_{1se} = 0.0573$, five genes retained non-zero coefficients: ALOX5, CXCR1, LPL, LTF, and TAC1 (Fig 3E). Subsequently, we constructed a random forest model (ntree = 1000, OOB = 0.0425). Based on feature importance evaluation (MeanDecreaseGini > 2), ALOX5 and CASP1 were selected. After intersecting the genes identified by both models, ALOX5 emerged as the only intersecting gene and was therefore identified as a potential pathogenic gene for DKD, which was used for further analysis (Fig 3F-H).

Differential expression and predictive performance of ALOX5 in DKD

To evaluate the expression characteristics of ALOX5 in diabetic kidney disease (DKD), we performed differential analysis and ROC performance assessment in both the training set and the independent validation set. In the training set, ALOX5 was significantly upregulated in DKD ($P < 0.005$), suggesting its potential involvement in the pathogenic process of DKD. We then validated this expression trend in two independent datasets, GSE47184 and GSE99325, where ALOX5 consistently exhibited upregulated expression (Fig 4A), further supporting its stable association with DKD.

To assess its potential value in identifying DKD subtypes with specific inflammatory characteristics, we conducted ROC analysis on ALOX5. In the training set, ALOX5 achieved an AUC of 0.994(95% CI: 0.981–1.000), demonstrating high discriminative performance in the discovery cohort. The two external validation datasets also showed good performance, with AUCs of 0.786(95% CI: 0.604–0.967). and 0.818(95% CI: 0.579–1.000)., respectively (Fig 4B). We further assessed model calibration using bootstrap internal validation (1000 resamples). The calibration plot suggested an overall good agreement between predicted and observed probabilities (Supplementary Fig. 3). These results indicate that ALOX5 exhibits stable and reproducible characteristics across different cohorts, supporting its potential as a biomarker for DKD.

Association of ALOX5 with immune regulation and clinical renal function

To explore the potential role of ALOX5 in diabetic kidney disease (DKD), we first analyzed its expression in relation to immune infiltration. The results showed that ALOX5 expression was significantly positively correlated with the infiltration of various pro-inflammatory immune cells, including monocytes (Fig 4C). Moreover, ALOX5 was positively correlated with M1 macrophage infiltration, while it exhibited a negative correlation with M2 macrophage infiltration, suggesting its close association with an inflammation-driven immune microenvironment.

To further investigate the biological processes that ALOX5 may influence, we conducted Gene Set Enrichment Analysis (GSEA) based on the Spearman correlation rankings between ALOX5 and the whole-genome expression. The GO analysis revealed that genes negatively correlated with ALOX5 were significantly enriched in metabolic pathways such as “small molecule catabolic process” and “organic acid catabolic process” (Fig 4D). KEGG analysis (Fig 4E) further indicated that ALOX5 expression was positively correlated with several immune activation-related pathways, including “MHC class I-mediated antigen processing and presentation.” These results suggest that high ALOX5 expression is associated with enhanced inflammatory immune characteristics and a trend of reduced metabolic activity, indicating its involvement in the formation of immune and metabolic imbalance in DKD.

To assess its clinical significance, we further validated our findings using the Nephroseq V5 database. ALOX5 expression showed a moderate negative correlation with glomerular filtration rate (GFR) ($P = 3.63 \times 10^{-2}$, $r = -0.634$), while it was positively correlated with serum creatinine (Cr) ($P = 1.08 \times 10^{-2}$, $r = 0.73$) (Fig 4F—G; Supplementary Table 7). These results suggest that elevated ALOX5 expression is associated with declining renal function in DKD and may participate in immune regulation and renal injury progression, indicating that its potential biological significance warrants further mechanistic investigation.

Single-cell analysis reveals activation of the 5-LOX pathway in pro-inflammatory macrophages

To further validate the expression patterns of core inflammation-related genes, we analyzed the expression of ALOX5 in the renal tissues of diabetic kidney disease patients using single-cell transcriptome data from GSE209781 (3 healthy controls and 3 DKD patients). After quality control and dimensionality reduction clustering, we identified a total of 40,801 cells in GSE209781. Based on typical marker genes, these cells were classified into 17 distinct cell clusters, allowing us to assess the expression levels of ALOX5 in different cell populations (Fig 5A). Notably, at the cellular level, ALOX5 expression was

elevated in immune-related cells such as T cells and B cells in DKD patients, with the most significant expression observed in macrophages (Fig 5B, D, E). This finding is consistent with observations from bulk RNA-seq analysis.

To further clarify the cellular heterogeneity of macrophages, we re-clustered the macrophage population into three subpopulations (Fig 5C; Supplementary Table 9). ALOX5 was expressed at higher levels in the $CD14^+$ monocyte and $CD86^+$ macrophage subpopulations, whereas the $CD163^+$ macrophage-associated subpopulation had limited cell numbers, and no statistically significant differences in ALOX5 expression were observed (Fig 5F). To further determine whether ALOX5 is involved in the state transition of macrophages, we constructed a single-cell pseudotime trajectory based on the three macrophage subpopulations mentioned above (Fig 5G). Although ALOX5 expression was relatively higher in $CD14^+$ monocytes and $CD86^+$ macrophages, its dynamic changes along the differentiation trajectory were not significant, suggesting that the expression level of ALOX5 may not be sufficient to reflect its pathway activation status.

While ALOX5 expression was relatively stable, its function relies on its interaction with ALOX5AP as an inflammatory switch. Thus, we further analyzed the expression patterns of ALOX5AP along the pseudotime trajectory (Fig 5H). The results showed a significant upward trend of ALOX5AP during the differentiation phase from $CD14^+$ monocytes to $CD86^+$ macrophages, which aligns with the emergence of a pro-inflammatory macrophage phenotype. To validate this single-cell observation, we subsequently performed multicolor immunohistochemical analysis to assess the spatial localization patterns of the ALOX5/ALOX5AP pathway in tissue samples.

mIHC confirms in situ activation of the 5-LOX pathway

Although single-cell analyses revealed the expression patterns and potential functional differences of ALOX5 and ALOX5AP in different macrophage subpopulations, RNA-level changes do not adequately reflect the spatial distribution at the protein level, nor do they determine whether these proteins are truly involved in pro-inflammatory processes within the tissue microenvironment. Therefore, to validate the actual localization and activation status of the 5-LOX pathway in renal tissues, we performed multicolor immunohistochemistry (mIHC) analysis, incorporating ALOX5, ALOX5AP, and macrophage-related inflammatory markers (Fig 6).

The results showed that both ALOX5 and its partner protein ALOX5AP exhibited prominent positive signals around the renal tubules and in the interstitial regions, with a high degree of co-localization with the macrophage marker CD68. This suggests that the 5-LOX pathway is primarily active in the infiltrating macrophages within the renal tissue.

Additionally, the pro-inflammatory macrophage phenotype markers iNOS and $NF-\kappa B$ also demonstrated significant positivity in the same regions, aligning closely with the spatial distribution of ALOX5 and ALOX5AP. The positive expression of the leukotriene receptor CYSLTR1 further suggests that downstream signals of the 5-LOX pathway may participate in local reactions within the microenvironment. Notably, CD163 staining did not show significant positivity, indicating a low proportion of $CD163^+$ macrophages in the tissue, which correlates with the limited numbers of $CD163^+$ macrophages observed in the single-cell analysis.For clearer visualization of colocalization, only representative protein combinations are shown in the main text, and the complete multichannel composite image has been moved to Supplementary Fig. 4.

Given the ethical limitations on obtaining normal renal biopsy tissues, we confirmed the low expression levels in normal controls using single-cell transcriptomics and validated these findings with references from the Human Protein Atlas (HPA). Due to differences in staining methods, this comparison is qualitative rather than quantitative. In the expression profiles of ALOX5, ALOX5AP, CD68, CYSLTR1, p65, iNOS, and CD163 in normal renal tissues, data from HPA indicated that these proteins are expressed at low levels or not expressed at all in normal renal tissues (Fig 7-8). In summary, the mIHC results support that the 5-LOX pathway is primarily localized in $CD68^+$ pro-inflammatory macrophage-related regions in the renal tissue. Furthermore, the upregulation of ALOX5AP is closely associated with an enhanced pro-inflammatory state of macrophages, providing direct histological evidence for the mechanisms suggested by single-cell analyses in this study.

Prediction of potential inhibitors for DKD

In order to further discover potential therapeutic agents for diabetic kidney disease (DKD), we initially utilized the Drug Signatures Database (DSigDB) for drug prediction and identified four candidate small molecules associated with DKD: Honokiol, Rev 5901, Quinacrine dihydrochloride, and caffeic acid. Subsequently, we performed molecular docking of these compounds with the ALOX5 protein to evaluate their binding capabilities and key binding sites. The docking results indicated that Rev 5901 exhibited the lowest binding energy (-8.5 kcal·mol^{-1}), suggesting it possesses the highest binding affinity among the four candidates. The predicted binding energies for Honokiol, Quinacrine, and caffeic acid were -7.6, -7.4, and -6.96 kcal·mol^{-1}, respectively.

Structural interaction analysis revealed that all four compounds can interact within the binding pocket of ALOX5. Honokiol (binding energy -7.6 kcal·mol^{-1}) was predicted to have close contact with the ARG-457 residue (with two proximity distances of approximately 2.5 Å), indicating the potential for forming stable polar/hydrogen-bond-like interactions, thereby stabilizing the ligand's conformation in the pocket (Fig 9A). Rev 5901 (binding energy -8.5 kcal·mol^{-1}) primarily maintains close interactions with ARG-370 (contact distance approximately 2.6–2.8 Å), a factor likely critical to its high affinity (Fig 9B).

Quinacrine dihydrochloride (binding energy -7.4 kcal·mol^{-1}) exhibited close contact with GLN-549 (around 2.5 Å), suggesting potential stabilization of the binding site through polar interactions (Fig 9C). Caffeic acid (binding energy -6.96 kcal·mol^{-1}) showed close contacts with several residues, including THR-545 (hydrogen bond distance approximately 1.9 Å) and contact with ARG-457, VAL-243, and LEU-448 at distances ranging from 2.3 to 3.4 Å, indicating that this small molecule may bind to the protein through multiple weak interactions (Fig 9D).

ADMET prediction and drug-likeness analysis

To assess the clinical translational potential of the selected arachidonic acid 5-lipoxygenase (ALOX5) binders, this study conducted a systematic evaluation of the physicochemical properties, pharmacokinetic features, and drug-like characteristics of four candidate compounds (Honokiol, Rev 5901, Quinacrine dihydrochloride (QNH), and caffeic acid) using the SwissADME platform . The relevant results are summarized in Table 1 , with complete data provided in Supplementary Table 8.

Among all candidates, Honokiol and the known ALOX5 inhibitor Rev 5901 exhibited the most favorable drug-like properties. Both compounds demonstrated high gastrointestinal absorption efficiency, indicating their suitability for development as oral formulations. Notably, they complied fully with Lipinski's Rule of Five, with no parameters exceeding the thresholds (molecular weight < 500, $\log P < 5$, number of hydrogen bond donors < 5, number of hydrogen bond acceptors < 10), displaying ideal physicochemical properties required for drug development. Additionally, Honokiol did not trigger any alerts for pan-assay interference compounds (PAINS), suggesting that its biological activity may be specific and less likely to be influenced by nonspecific experimental interference. In contrast, while caffeic acid also demonstrated high predicted gastrointestinal absorption efficiency and adhered to Lipinski's Rule of Five, it triggered PAINS alerts due to the presence of a catechol structure, which could pose predicted risks of chemical instability or nonspecific reactions. Quinacrine hydrochloride showed the least favorable predicted profile overall: it not only had a predicted low gastrointestinal absorption efficiency but also violated Lipinski's Rule of Five (logP > 4.15). Furthermore, its aminoacridine structure triggered PAINS alerts.

In conclusion, the analysis of absorption, distribution, metabolism, excretion, and toxicity (ADMET) characteristics suggests that Honokiol is a potential inhibitor with favorable predicted oral bioavailability and potential structural specificity, showing a computational profile similar to the positive control drug Rev 5901, though further experimental validation is warranted.

Discussion

Diabetic kidney disease (DKD) is a leading cause of end-stage kidney disease, and effective options to halt tubulointerstitial inflammation remain limited. Recent tumor immune microenvironment (TIME) studies illustrate how immune-cell heterogeneity and multi-omics signatures can inform therapeutic decision-making[10,11]; this analytical framework provides useful methodological parallels for dissecting the inflammatory milieu in DKD. In this study, we combined weighted gene co-expression network analysis (WGCNA) with machine-learning feature selection to prioritize ALOX5 as a DKD-associated inflammatory gene. Higher ALOX5 expression was associated with worse renal function (reduced eGFR and increased serum creatinine) and a more pro-inflammatory immune landscape. Integrating single-cell transcriptomes with trajectory inference, we observed increased ALOX5AP (FLAP) expression along an inferred monocyte-to-macrophage continuum, supporting a model in which leukotriene biosynthesis may be reinforced during macrophage differentiation. Multi-color immunohistochemistry provided spatial evidence for ALOX5/ALOX5AP co-localization in infiltrating interstitial macrophages. Finally, molecular docking and SwissADME analyses were used to prioritize candidate inhibitors (e.g., honokiol) for future experimental validation.

Recent studies suggest that glomerular injury may not be the sole determining factor or primary event in the progression of DKD. Increasing evidence points to tubular injuries, particularly proximal tubular damage, playing a significant role in the occurrence and development of DKD. As a result, the focus has shifted partly from glomerular lesions to tubular injury[12,13]. In the renal tubular interstitial microenvironment, inflammatory pathways play a central role in the progression of DKD[14]. Consistent with our immune infiltration analysis, previous research has confirmed that the immune microenvironment of DKD is predominantly composed of myeloid cells, particularly the infiltration of monocytes and macrophages[15,16]. These infiltrating macrophages are not mere bystanders; they actively participate in tissue damage and fibrosis. Macrophages secrete various cytokines, including M1-type pro-inflammatory cytokines (such as TNF-α, IL-6, IL-23) and chemokines (such as MCP1, CCL2). M2 macrophages release anti-inflammatory cytokines (such as IL-10), pro-fibrotic factors (such as TGF-β), and chemokines (CCL17, CCL18, and CCL22)[17,18]. In a high-glucose environment, macrophages act as the primary phagocytic cells of the innate immune system, activating Toll-like receptors (TLRs) through endogenous damage-associated molecular patterns (DAMPs) and inducing renal tubular interstitial inflammatory responses via the NF-κB signaling pathway[19]. This process not only triggers the release of pro-inflammatory factors such as TNF-α and IL-1β but, crucially, the NF-κB pathway in turn enhances the secretion of chemokine CCR2, promoting the infiltration of inflammatory cells and the transformation of M1 macrophages, thereby establishing a "recruitment-activation-re-recruitment" cycle of vicious cycle inflammation[20]; see Fig. 10. However, the key molecular switch that initiates and maintains this inflammatory cycle has long remained insufficiently elucidated, providing an important scientific entry point for research.

Our study fills this gap by identifying ALOX5 as a crucial node linking metabolic dysregulation and immune imbalance[21,22]. ALOX5, a member of the ALOX family, is responsible for the oxidative metabolism of polyunsaturated fatty acids and is the rate-limiting enzyme in the synthesis of leukotrienes (LTs), which are key mediators of inflammation. However, mere expression of the enzyme is not sufficient to trigger inflammation; the presence of the activating protein ALOX5AP is vital for delivering substrates to ALOX5[23,24]. Our single-cell pseudo-time analysis indicates that, although ALOX5 is significantly overexpressed at the tissue level in DKD, its cofactor ALOX5AP is the key player in the differentiation trajectory of monocytes into pro-inflammatory macrophages. This suggests that as monocytes differentiate, the induced expression of ALOX5AP may activate ALOX5 enzymatic activity, thus initiating leukotriene synthesis. This inference is supported by spatial evidence from our mIHC experiments, which showed high co-localization of ALOX5 and its auxiliary protein FLAP (ALOX5AP) in $CD68^+$ macrophages, indicating these cells are central sources for local leukotriene synthesis in the kidney interstitium, potentially driving inflammation amplification. Further mechanistic analysis revealed that $CD68^+$ macrophages and damaged tubular epithelial cells co-express CYSLTR1, suggesting that these infiltrating macrophages not only produce leukotrienes (e.g., LTC_4/LTD_4) but may also amplify inflammation via autocrine or paracrine signaling through $CysLT_1$ receptors.

Previous research indicates that the leukotriene-CYSLTR1 axis can promote macrophage recruitment, cytokine release, and fibrotic processes, aligning with our hypothesis[25,26]. Notably, p65 (NF-κB) and iNOS show strong co-localization in $ALOX5^+/CD68^+$ macrophages, indicating these cells are in a typical pro-inflammatory state. The activation of the NF-κB signaling pathway is a central route for inducing iNOS expression and inflammatory mediator release, while the leukotriene pathway is thought to further enhance the extent of NF-κB activation. Therefore, we speculate that leukotriene production induced by ALOX5–FLAP may be involved in activating the NF-κB/p65–iNOS signaling pathway, thereby promoting macrophage polarization to the pro-inflammatory phenotype and exacerbating renal tubular interstitial inflammation. Previous studies have also supported this viewpoint, demonstrating that ALOX5 and its metabolic products can activate NF-κB in cells. Inhibition of ALOX5AP/FLAP or knockdown of Alox5 can suppress NF-κB activation and diminish M1 polarization. Together, these evidences indicate that ALOX5 could be a critical node in the inflammatory response of macrophages in DKD, thus representing a potential intervention target[27–29].

Given the role of ALOX5 in the immune microenvironment imbalance of DKD, pharmacological interventions targeting this molecule may hold significant clinical translational value. Through molecular docking analysis, we selected Honokiol, Rev 5901, Quinacrine dihydrochloride, and caffeic acid as potential high-affinity inhibitors of ALOX5. Rev 5901, already known as a specific 5-LOX inhibitor, supports the rationale of identifying ALOX5 as a druggable target[30,31]. Honokiol, a natural polyphenolic compound, has previously been reported to exhibit significant dual anti-inflammatory and antioxidant activities while blocking ALOX5-mediated leukotriene synthesis. Considering DKD is a disease characterized by coexisting metabolic and immune dysregulation, Honokiol may counteract the inflammatory cascade mediated by ALOX5 and high-glucose-induced oxidative stress[32,33]. This opens a novel and promising strategy for developing new therapies for DKD based on natural products.

Although this study emphasizes the importance of ALOX5 in DKD, several limitations must be acknowledged. First, the findings mainly rely on multi-cohort bioinformatics analyses; while they are reliable, further validation in larger clinical patient cohorts is necessary. Second, although single-cell sequencing and mIHC provide static evidence for cell polarization and co-localization in situ, functional loss experiments in cellular or animal models involving ALOX5 gene knockout or inhibitor intervention are still lacking, warranting future exploration of how the ALOX5 signaling pathway evolves over time and interacts with other pathways (such as metabolic pathways in tubular cells). Lastly, molecular docking and SwissADME provide only structural predictions for potential inhibitors; their pharmacodynamics, pharmacokinetic properties, and clinical efficacy still need rigorous evaluation in subsequent functional studies and clinical trials.

Despite the current lack of in vivo functional validation using gene knockout models, we ensured the robustness and reliability of our analytical results through rigorous multi-omics integration and multi-color immunohistochemistry (mIHC) in situ spatial verification. Future studies will further validate the causal role of the ALOX5/ALOX5AP pathway in DKD through functional experiments.

In summary, this study suggests ALOX5 as a robust biomarker for tubular injury in DKD through multi-omics integrative analysis. Mechanistically, we findings suggest that leukotrienes mediated by ALOX5–ALOX5AP may act as upstream signals activating the NF-κB/iNOS signaling pathway, thereby promoting kidney injury via inflammatory macrophages. These findings not only deepen our understanding of the mechanisms behind tubular interstitial inflammation in DKD but also provide new potential therapeutic strategies to address global health challenges.

Methods

Data Collection and Preparation

Gene expression profiles of diabetic kidney disease (DKD) were obtained from the Gene Expression Omnibus (GEO, http://www.ncbi.nlm.nih.gov/geo). Four microarray datasets were included: GSE30529 (GPL571; 9 DKD and 12

control; tubules)[34], GSE104954 (GPL22945; 7 DKD and 18 control; tubules)[35], GSE47184 (GPL14663; 11 DKD and 4 control; tubules)[36], and GSE99325 (GPL19184; 18 DKD and 7 control; tubules)[37]. Series matrix files were downloaded and preprocessed within each dataset by mapping probe IDs to official gene symbols using platform annotations; for genes with multiple probes, the median expression value was retained. Expression values were $\log_2$-transformed when necessary and quantile-normalized prior to cross-dataset integration. GSE104954 and GSE30529 were merged by common gene symbols to construct the training cohort (16 DKD and 30 control samples), and batch effects attributable to study origin were corrected using `ComBat` (`sva` package) with disease status (DKD vs control) included as a biological covariate to avoid removal of phenotype-related signals; correction performance was evaluated using PCA and distributional checks (box plots) before and after adjustment (Supplementary Fig. 1). GSE47184 (11 DKD, 4 control) and GSE99325 (18 DKD, 7 control) were used as independent external validation cohorts to assess expression patterns and diagnostic performance of core genes. In addition, the single-cell RNA-seq dataset GSE209781 (GPL24676; 3 DKD and 3 normal; renal cortex)[38] was used to characterize cell-type localization and expression patterns. Tissue types (tubules/tubules/renal cortex) were determined according to GEO sample annotations and the original publications, and detailed dataset information is provided in Supplementary Table 1.

Weighted gene co-expression network analysis (WGCNA)

We used the R package WGCNA to construct a weighted gene co-expression network aimed at identifying key co-expression modules and potential hub genes associated with the DKD phenotype[39]. First, we performed hierarchical clustering on all samples in the discovery cohort to detect potential outliers, and no significant outliers were observed. Next, we evaluated the scale-free R^2 and average connectivity under different soft-thresholding powers (β) based on the scale-free topology criterion, ultimately selecting $R^2 = 0.9$ and $\beta = 10$ as the optimal soft-threshold values for constructing the scale-free network. Subsequently, we calculated the similarity between genes based on the topological overlap matrix (TOM) and identified initial modules using the Dynamic Tree Cut method. To reduce module redundancy, we further merged modules based on the correlation between module eigengenes (MEs), setting the merging threshold at cutHeight = 0.25. In total, five stable co-expression modules were identified.

Identification of differentially expressed inflammation-related genes (DEG-IRGs) in DKD

Differential expression analysis was performed in the discovery cohort using the `limma` package with linear models and empirical Bayes moderation. Genes with $|\log_2 \mathrm{FC}| > 1$ and FDR-adjusted $P < 0.05$ were defined as differentially expressed genes (DEGs). In parallel, we extracted genes from the DKD-associated WGCNA module (turquoise module) that showed the strongest correlation with the DKD phenotype. In addition, inflammation-related genes were retrieved from GeneCards using the keyword “Inflammation” and filtered by a relevance score ≥ 7 (Supplementary Table 2). The intersection of DEGs, turquoise-module genes, and GeneCards inflammation genes was defined as differentially expressed inflammation-related genes (DEG-IRGs) and visualized using the `VennDiagram` package[40]. This three-way intersection strategy was designed to reduce false positives and enhance biological relevance by retaining genes that (i) show DKD-associated transcriptional changes (DEGs), (ii) reside within a phenotype-associated co-expression network module (WGCNA), and (iii) are supported by prior knowledge as inflammation-related (GeneCards).The purpose of this step was to prioritize candidate biomarkers with discriminatory utility from the biologically constrained DEG-IRG set, rather than to identify hub genes solely on the basis of network topology. Therefore, WGCNA was used to define disease-relevant co-expression context, whereas subsequent LASSO and random forest analyses were used for the final feature selection and robustness screening.

Functional enrichment analysis of DEG-IRGs

We performed gene ontology (GO) enrichment analysis and Kyoto Encyclopedia of Genes and Genomes (KEGG) pathway analysis on the selected differentially expressed inflammation-related genes (DEG-IRGs) using the R package clusterProfiler to explore their potential biological functions and associated signaling pathways[41,42]. The GO enrichment analysis encompassed three functional categories: biological process (BP), molecular function (MF), and cellular component (CC)[43]. We then utilized ggplot2 to display the top ten significantly enriched entries for each analysis.

Immune cell infiltration analysis

By applying xCell to microarray data, we can obtain the estimated proportions of immune cell and stromal cell types in each DKD sample. The effective statistical significance threshold for cellular analysis is set at $p < 0.05$. The cell types are categorized into lymphocytes and myeloid cells. To clarify the interactions between immune cells and inflammation, and to explore key immune cells involved in the pathogenesis of DKD, we identified co-expression patterns based on Spearman correlation analysis[44].

Identification of core genes using machine learning

To further identify key inflammation-related genes in DKD, we applied two machine learning algorithms—Random Forest (RF) and Least Absolute Shrinkage and Selection Operator (LASSO) regression—on the selected differentially expressed inflammation-related genes (DEG-IRGs). First, we constructed a Random Forest model using the R package randomForest (ntree = 1000, setting a seed for result reproducibility). The importance of the genes was assessed based on the MeanDecreaseGini metric, and the top-ranked genes were selected as candidate variables. Next, we performed LASSO regression analysis on the same gene set using the R package glmnet. The optimal regularization parameter λ was determined through 10-fold cross-validation, and feature genes were selected based on λ.1se to obtain a feature set with improved generalizability. Finally, the intersection of the feature genes identified by both algorithms was taken as the candidate biomarker genes associated with DKD[45,46].

Expression analysis and evaluation of candidate biomarkers

To validate the differential expression of the identified core genes, we extracted their normalized expression matrices from independent external datasets (GSE47184 and GSE99325). We compared expression levels between the DKD and control groups using a two-tailed Wilcoxon rank-sum test (`wilcox.test`, $P < 0.05$). The distribution of expression levels and the significance of differences were visualized using boxplots created with the R package `ggplot2`.

To assess the diagnostic performance of the core genes, receiver operating characteristic (ROC) curves were generated for both the training set and the external validation sets (GSE47184 and GSE99325) using the R package `pROC`[47]. The area under the curve (AUC) along with its 95% confidence interval (CI) was calculated to quantify predictive accuracy. According to commonly accepted standards, an AUC > 0.7 indicates good discriminatory performance.

Furthermore, to evaluate the agreement between predicted and observed probabilities, a logistic regression model was constructed using the R package `rms`[48]. Model calibration was assessed by plotting a calibration curve with internal validation via bootstrap resampling (1000 iterations).

Correlation analysis between ALOX5 and immune characteristics

To assess the relationship between ALOX5 expression levels and the immune infiltration status in kidney tissues, this study utilized relative abundances of various immune cell types (enrichment scores) calculated based on the xCell algorithm. A two-tailed Spearman correlation analysis was performed to compute the correlation coefficients between ALOX5 and the scores of each immune cell type, with statistical significance set at $P < 0.05$. The correlation results were visualized using the R packages ggplot2 and corrplot to illustrate the correlation and significance between ALOX5 and different immune cell types.

Clinical correlation analysis of ALOX5

The NephroseqV5 database is a genomic data platform focused on kidney disease research, used to explore the relationship between ALOX5 and renal function (`https://www.nephroseq.org`). The expression data for ALOX5 were downloaded from the NephroseqV5 database, which provides transcriptomic data related to diabetic kidney disease. We conducted a correlation analysis between the downloaded ALOX5 expression data and renal function parameters. Spearman correlation analysis was employed to investigate the potential associations between the expression levels of the core gene and various renal function metrics. Scatter plots were generated using the ggplot2 package in R to visually represent these relationships[49].

Gene set enrichment analysis (GSEA)

To evaluate the correlation of the ALOX5 gene with the entire transcriptome, we conducted gene set enrichment analysis (GSEA) on the list of genes sorted by their correlation with ALOX5. First, we calculated the Spearman correlation coefficients and their significance between ALOX5 and all other genes. The Spearman correlation coefficient for each gene was used as a ranking statistic to construct a gene list (geneList) with gene symbols (SYMBOL) as row names, sorted in descending order based on the correlation coefficients. We performed enrichment analysis on the sorted gene list using pre-downloaded gene set files (c5.go.v2025.1.Hs.symbols.gmt, c2.cp.kegg_medicus.v2025.1.Hs.symbols.gmt)[50]. This analysis allowed us to identify biological processes and pathways associated with the expression of ALOX5 in the context of the entire transcriptome.

scRNA-seq data processing and pseudotime analysis

In this study, we obtained the raw single-cell RNA sequencing (scRNA-seq) data from the GEO database (GSE209781) and processed it using the Seurat R package. To ensure data quality, we set the parameters such that features for individual cells were greater than 500 and less than 5000, with mitochondrial gene content below 50%[51]. Ultimately, 40,801 cells were included for further analysis. To identify highly variable genes, we utilized the FindVariableFeatures function and generated a feature gene scatter plot. Subsequently, the data were normalized using NormalizeData and ScaleData, followed by principal component analysis (PCA) based on the high-variable genes, selecting the top 20 principal components for subsequent analysis. To eliminate batch effects among different samples, we applied the Harmony algorithm (RunHarmony) to correct the PCA

results. For clustering analysis, we employed the FindNeighbors and FindClusters functions, performing clustering at various resolution parameters (0.2, 0.4, 0.6, 0.8, 1.0, and 1.2), and selected a resolution of 0.4 based on the clustree constructed. Finally, we utilized UMAP for non-linear dimensionality reduction visualization. The annotation of cell types was based on gene expression profiles reported in previous research (Supplementary Fig. 2). To identify subtypes of immune cells (macrophages), we extracted the cell types and conducted a second round of clustering using the same procedures as the first round. We then annotated the clusters obtained from the reclustering. To investigate the temporal dynamics of the cell populations, trajectory analysis was conducted to reconstruct changes over time, allowing us to infer cellular evolution and differentiation at the single-cell level. To explore the differentiation and developmental trajectories of specific cell subtypes, we performed rigorous analysis using the "monocle3" R package[52].

Patient Recruitment and Sample Collection

This study included kidney biopsy samples from three patients diagnosed with diabetic kidney disease (DKD) . The inclusion criteria were as follows: patients aged 18 years or older, diagnosed with type 2 diabetes according to the WHO 1999 diabetes diagnostic criteria and classification system for diabetes etiology, and who voluntarily signed informed consent; and those diagnosed with DKD based on pathological examination, which indicated lesions in the glomeruli, renal tubules, and renal interstitium. Exclusion criteria included: patients with type 1 diabetes; those with a history of non-diabetic kidney disease (NDKD) or who had concurrent NDKD; individuals with a history of organ or bone marrow transplantation; and pregnant or breastfeeding women.

Multiplex Immunohistochemistry (mIHC)

First, 4-micron thick formalin-fixed paraffin-embedded (FFPE) kidney tissue sections were prepared and deparaffinized with xylene, followed by hydration through a series of graded ethanol solutions. Antigen retrieval was performed using a microwave heating method in EDTA buffered solution (pH 8.0). After cooling, endogenous peroxidase activity was blocked with 3% hydrogen peroxide solution for 15 minutes, followed by a 30-minute incubation at room temperature with 10% normal goat serum for further blocking. Multiplex immunofluorescence staining was conducted using the sequential tyramide signal amplification (TSA) protocol provided by Hunan Aifang Biotechnology Co., Ltd. (AFBio). During each staining cycle, the sections were incubated overnight at 4 °C with the primary antibodies listed as follows: inducible nitric oxide synthase (iNOS) antibody (1:300, AFBio, China, AFRP0001), 5-lipoxygenase activating protein (ALOX5AP) antibody (1:400, Bioss, China, BS-7556R), cysteinyl leukotriene receptor 1 (CYSLTR1) antibody (1:400, Bioss, China, BS-14168R), CD163 antibody (1:500, AFBio, China, AFRM0015), 5-lipoxygenase (ALOX5) antibody (1:400, Immunoway, USA, YT0027), nuclear factor kappa B p65 (NF-κB p65) antibody (1:500, AFBio, China, AFRM0286), and CD68 antibody (1:500, AFBio, China, AF20022). After washing with PBST, the sections were incubated at room temperature for 30 minutes with the HRP-conjugated polymer secondary antibodies (anti-rabbit/anti-mouse). Subsequently, TSA fluorescent dye working solution (TRY-570, TYR-520, TYR-620, TYR-650, TYR-480, TYR-690, TYR-780; AFBio, China) was added and incubated for 3 to 10 minutes to complete the deposition of the fluorophores. Following the signal development, to prevent cross-reactivity in subsequent staining cycles, the antibody-enzyme complexes were stripped using microwave treatment in the antigen retrieval buffer. This procedure was repeated until all target markers were labeled. After completing all staining cycles, nuclei were counterstained with DAPI for 10 minutes, and the sections were mounted with an anti-fade mounting medium. Fluorescent images were captured using a laser scanning confocal microscope.

Validation of Protein Expression in Normal Human Kidney

To validate the protein expression levels of ALOX5, ALOX5AP, and other key markers in normal kidney tissue, we retrieved immunohistochemistry (IHC) images from the Human Protein Atlas (HPA) database (https://www.proteinatlas.org/).

Candidate drug prediction and molecular docking

The Drug Signatures Database (DSigDB) is a resource that identifies associations between drugs, chemicals, and target genes. The database contains 22,527 genes and 17,389 unique compounds. Evaluating the interactions between drugs and proteins is crucial for developing potential therapeutic agents. To screen for potential regulatory compounds related to ALOX5, we first utilized the Enrichr online tool suite (https://maayanlab.cloud/modEnrichr/) and selected DSigDB for drug-gene enrichment analysis. ALOX5 was input as the target gene to obtain significantly associated candidate compounds from DSigDB (Supplementary Table 3). Four candidate compounds were retrieved from PubChem (https://pubchem.ncbi.nlm.nih.gov/): Honokiol (PubChem CID: 72303), Rev 5901 (PubChem CID: 5059), Quinacrine Dihydrochloride (PubChem CID: 6239), and Caffeic acid (PubChem CID: 689043). Subsequently, to assess the binding capability of these small molecules with ALOX5, molecular docking analysis was performed using AutoDock Vina. The three-dimensional structure of ALOX5 was obtained from the Protein Data Bank (PDB) (PDB ID: pdb_00003o8y). The

three-dimensional structures of the small molecules were downloaded from PubChem and constructed using ChemBio3D, followed by energy minimization using the MM2 force field. The preparation of the protein structure included the removal of ligands and water molecules, completion of missing amino acids, hydrogen addition, and conversion to PDBQT format using AutoDockTools. The ligand structures were also converted to PDBQT format within AutoDockTools. The docking active pocket was designed to cover the catalytic center region. Docking was executed using AutoDock Vina with default parameters (exhaustiveness = 8). After docking completion, the conformation with the lowest binding energy was selected as the optimal binding model, and the protein-ligand complex was visualized using PyMOL.

ADMET prediction and drug-likeness analysis

In this study, we utilized the SwissADME online platform (http://www.swissadme.ch) to evaluate the pharmacokinetic properties and drug-likeness of the screened ALOX5 small molecule ligands (Honokiol, Rev 5901, Quinacrine Dihydrochloride, and Caffeic acid). First, we retrieved and downloaded the canonical SMILES sequences for these four compounds from the PubChem database. The SMILES sequences were then imported into the SwissADME server for calculations. This research focused on assessing the following parameters: (1) physicochemical properties and compliance with Lipinski's Rule of Five, which includes molecular weight (MW), the octanol-water partition coefficient (LogP), and the number of hydrogen bond donors (HBD) and acceptors (HBA) to predict the druglikeness of the compounds; (2) pharmacokinetic characteristics, primarily evaluating gastrointestinal (GI) absorption efficiency; and (3) medicinal chemistry characteristics, using the pan-assay interference compounds (PAINS) alert filter to assess whether the compounds possess potential non-specific reactive structures.

Statistical analysis

Intergroup comparisons were conducted using the Wilcoxon rank-sum test, implemented through the wilcox.test() function in R. The significance levels were visualized using the conventional asterisk system ($p < 0.05$; $p < 0.01$; $p < 0.001$; $p < 0.0001$; n.s., not significant), with annotations added using the ggpubr package (stat_compare_means()). All statistical analyses and visualizations were carried out in R.

References

1. Tziomalos, K. & Athyros, V. G. Diabetic nephropathy: new risk factors and improvements in diagnosis. *The review diabetic studies: RDS* **12**, 110 (2015).
2. Alicic, R. Z., Rooney, M. T. & Tuttle, K. R. Diabetic kidney disease: challenges, progress, and possibilities. *Clin. journal Am. Soc. Nephrol.* **12**, 2032–2045 (2017).
3. Pan, X. *et al.* The burden of diabetes-related chronic kidney disease in china from 1990 to 2019. *Front. endocrinology* **13**, 892860 (2022).
4. de Boer, I. H. *et al.* Diabetes management in chronic kidney disease: a consensus report by the american diabetes association (ada) and kidney disease: Improving global outcomes (kdigo). *Diabetes care* **45**, 3075–3090 (2022).
5. Tuttle, K. R. *et al.* Molecular mechanisms and therapeutic targets for diabetic kidney disease. *Kidney international* **102**, 248–260 (2022).
6. Mori, Y. *et al.* Kim-1 mediates fatty acid uptake by renal tubular cells to promote progressive diabetic kidney disease. *Cell metabolism* **33**, 1042–1061 (2021).
7. Wang, X. *et al.* The role of tubulointerstitial markers in differential diagnosis and prognosis in patients with type 2 diabetes and biopsy proven diabetic kidney disease. *Clin. chimica acta* **547**, 117448 (2023).
8. Williams, B., Cliff, C. L., Lee, K., Squires, P. & Hills, C. The role of the nlrp3 inflammasome in mediating glomerular and tubular injury in diabetic nephropathy. *Front. physiology* **13**, 907504 (2022).
9. Aranda-Rivera, A. K. *et al.* Involvement of inflammasome components in kidney disease. *Antioxidants* **11**, 246 (2022).
10. Xia, W. *et al.* Molecular subtypes and prognostic signature rooted in disulfidptosis highlight tumor microenvironment in lung adenocarcinoma. *Chin. J. Cancer Res.* **37**, 796 (2025).
11. Zhang, P. *et al.* Metabolic reprogramming signature predicts immunotherapy efficacy in lung adenocarcinoma: Targeting slc25a1 to overcome immune resistance. *Chin. J. Cancer Res.* **37**, 1000 (2025).
12. Yao, L. *et al.* Mitochondrial dysfunction in diabetic tubulopathy. *Metabolism* **131**, 155195 (2022).
13. Gilbert, R. E. Proximal tubulopathy: prime mover and key therapeutic target in diabetic kidney disease. *Diabetes* **66**, 791–800 (2017).
14. Wada, J. & Makino, H. Inflammation and the pathogenesis of diabetic nephropathy. *Clin. science* **124**, 139–152 (2013).

15. Youssef, N., Noureldein, M. H., Riachi, M. E., Haddad, A. & Eid, A. A. Macrophage polarization and signaling in diabetic kidney disease: a catalyst for disease progression. *Am. J. Physiol. Physiol.* **326**, F301–F312 (2024).

16. Klessens, C. Q. *et al.* Macrophages in diabetic nephropathy in patients with type 2 diabetes. *Nephrol. Dial. Transplantation* **32**, 1322–1329 (2017).

17. Li, H.-D. *et al.* Roles and crosstalks of macrophages in diabetic nephropathy. *Front. Immunol.* **13**, 1015142 (2022).

18. Cantero-Navarro, E. *et al.* Role of macrophages and related cytokines in kidney disease. *Front. medicine* **8**, 688060 (2021).

19. Koc, M. *et al.* Toll-like receptor expression in monocytes in patients with chronic kidney disease and haemodialysis: relation with inflammation. *Nephrol. Dial. Transplantation* **26**, 955–963 (2011).

20. Ito, S. *et al.* Effects of a ccr2 antagonist on macrophages and toll-like receptor 9 expression in a mouse model of diabetic nephropathy. *Am. J. Physiol. Physiol.* **321**, F757–F770 (2021).

21. Luo, M., Jones, S. M., Peters-Golden, M. & Brock, T. G. Nuclear localization of 5-lipoxygenase as a determinant of leukotriene b4 synthetic capacity. *Proc. Natl. Acad. Sci.* **100**, 12165–12170 (2003).

22. Funk, C. D. Prostaglandins and leukotrienes: advances in eicosanoid biology. *science* **294**, 1871–1875 (2001).

23. Crosslin, D. R. *et al.* Genetic effects in the leukotriene biosynthesis pathway and association with atherosclerosis. *Hum. genetics* **125**, 217–229 (2009).

24. Dixon, R. *et al.* Requirement of a 5-lipoxygenase-activating protein for leukotriene synthesis. *Nature* **343**, 282–284 (1990).

25. Ichiyama, T. *et al.* Cysteinyl leukotrienes induce monocyte chemoattractant protein 1 in human monocytes/macrophages. *Clin. & Exp. Allergy* **35**, 1214–1219 (2005).

26. Haneda, Y. *et al.* Leukotriene d4 enhances tumor necrosis factor-α-induced vascular endothelial growth factor production in human monocytes/macrophages. *Cytokine* **55**, 24–28 (2011).

27. Otunctemur, A. *et al.* Beneficial effects montelukast, cysteinyl-leukotriene receptor antagonist, on renal damage after unilateral ureteral obstruction in rats. *Int. braz j urol* **41**, 279–287 (2015).

28. Chen, X., Xie, H., Liu, Y., Ou, Q. & Deng, S. Interference of alox5 alleviates inflammation and fibrosis in high glucose-induced renal mesangial cells. *Exp. Ther. Medicine* **25**, 34 (2022).

29. Lim, C. S., Veltri, B., Kashon, M., Porter, D. W. & Ma, Q. Multi-walled carbon nanotubes induce arachidonate 5-lipoxygenase expression and enhance the polarization and function of m1 macrophages in vitro. *Nanotoxicology* **17**, 249–269 (2023).

30. Hoque, A. *et al.* Increased 5-lipoxygenase expression and induction of apoptosis by its inhibitors in esophageal cancer: a potential target for prevention. *Carcinogenesis* **26**, 785–791 (2005).

31. Tennant, C. M., Seale, J. P. & Temple, D. M. Effects of a 5-lipoxygenase inhibitor, rev-5901, on leukotriene and histamine release from human lung tissue in-vitro. *J. pharmacy pharmacology* **39**, 309–311 (1987).

32. Tse, A. K.-W., Wan, C.-K., Shen, X.-L., Yang, M. & Fong, W.-F. Honokiol inhibits tnf-α-stimulated nf-κb activation and nf-κb-regulated gene expression through suppression of ikk activation. *Biochem. pharmacology* **70**, 1443–1457 (2005).

33. Hamasaki, Y. *et al.* Inhibition of leukotriene synthesis by honokiol in rat basophilic leukemia cells. *Int. archives allergy immunology* **110**, 278–281 (1996).

34. Woroniecka, K. I. *et al.* Transcriptome analysis of human diabetic kidney disease. *Diabetes* **60**, 2354–2369 (2011).

35. Grayson, P. C. *et al.* Metabolic pathways and immunometabolism in rare kidney diseases. *Annals rheumatic diseases* **77**, 1226–1233 (2018).

36. Ju, W. *et al.* Defining cell-type specificity at the transcriptional level in human disease. *Genome research* **23**, 1862–1873 (2013).

37. Shved, N. *et al.* Transcriptome-based network analysis reveals renal cell type-specific dysregulation of hypoxia-associated transcripts. *Sci. reports* **7**, 8576 (2017).

38. Lv, Z. *et al.* Trail induces podocyte panoptosis via death receptor 5 in diabetic kidney disease. *Kidney Int.* **107**, 317–331 (2025).

39. Langfelder, P. & Horvath, S. Wgcna: an r package for weighted correlation network analysis. *BMC bioinformatics* **9**, 559 (2008).

40. Chen, H. & Boutros, P. C. Venndiagram: a package for the generation of highly-customizable venn and euler diagrams in r. *BMC bioinformatics* **12**, 35 (2011).

41. Yu, G., Wang, L.-G., Han, Y. & He, Q.-Y. clusterprofiler: an r package for comparing biological themes among gene clusters. *Omics: a journal integrative biology* **16**, 284–287 (2012).

42. Kanehisa, M. & Goto, S. Kegg: kyoto encyclopedia of genes and genomes. *Nucleic acids research* **28**, 27–30 (2000).

43. The gene ontology resource: enriching a gold mine. *Nucleic acids research* **49**, D325–D334 (2021).

44. Aran, D., Hu, Z. & Butte, A. J. xcell: digitally portraying the tissue cellular heterogeneity landscape. *Genome biology* **18**, 220 (2017).

45. Friedman, J. H., Hastie, T. & Tibshirani, R. Regularization paths for generalized linear models via coordinate descent. *J. statistical software* **33**, 1–22 (2010).

46. Sarica, A., Cerasa, A. & Quattrone, A. Random forest algorithm for the classification of neuroimaging data in alzheimer's disease: a systematic review. *Front. aging neuroscience* **9**, 329 (2017).

47. Robin, X. *et al.* proc: an open-source package for r and s+ to analyze and compare roc curves. *BMC bioinformatics* **12**, 77 (2011).

48. Harrell Jr, F. E., Lee, K. L. & Mark, D. B. Multivariable prognostic models: issues in developing models, evaluating assumptions and adequacy, and measuring and reducing errors. *Stat. medicine* **15**, 361–387 (1996).

49. Tang, R. *et al.* Single-cell transcriptomics uncover hub genes and cell–cell crosstalk in patients with hypertensive nephropathy. *Int. Immunopharmacol.* **125**, 111104 (2023).

50. Liberzon, A. *et al.* The molecular signatures database hallmark gene set collection. *Cell systems* **1**, 417–425 (2015).

51. Lake, B. B. *et al.* An atlas of healthy and injured cell states and niches in the human kidney. *Nature* **619**, 585–594 (2023).

52. Trapnell, C. *et al.* The dynamics and regulators of cell fate decisions are revealed by pseudotemporal ordering of single cells. *Nat. biotechnology* **32**, 381–386 (2014).

Acknowledgements

We are grateful to Guizhou University and Guizhou Provincial People's Hospital for providing the valuable research platform and support during the course of this study.

Ethics approval and consent to participate

All kidney biopsy samples were collected after obtaining informed consent from the patients. This study was approved by the Ethics Committee of Guizhou Provincial People's Hospital (Approval No: 2022-65) and was conducted in strict accordance with the Declaration of Helsinki and relevant ethical guidelines for human research.

Author contributions statement

W.L. and Y.D. conceived and designed the study. Y.Z. and J.Y. supervised the project and acquired funding. W.L., Y.D., and Q.X. developed the methodology. W.L., L.Z., Y.Z., and J.Y. designed the bioinformatics analyses. W.L., L.Z., Y.Z., and X.X. performed data processing, statistical analyses, and visualization. Y.D., L.L., and F.Y. curated the data and assisted with validation. Y.Z., J.Y., D.A., and L.L. coordinated patient recruitment and sample collection. W.L., Y.D., D.Y., K.Y., and D.A. performed the multiplex immunohistochemistry experiments. X.L. and L.J.L. provided technical support for imaging and interpretation. W.L. drafted the manuscript. Y.D., Y.Z., and J.Y. revised the manuscript. All authors reviewed and approved the final manuscript.

Additional information

Competing interests: The authors declare no competing interests.

Data availability

The datasets generated and analyzed during the current study are available in the GEO repository (Accession numbers: GSE104954, GSE30529, GSE47184, GSE99325, GSE209781). Requests for additional data or materials should be directed to J.Y. (email: yuanjinger@126.com).

Funding

This work was supported by the National Natural Science Foundation of China (Grant Nos. 82360148);Guizhou Science & Technology Department (Grant No. QKHCG2023-ZD010); Talent Fund of Guizhou Provincial People's Hospital (Grant No. [2022]-1); Guizhou Provincial People's Hospital Research Fund, Youth Fund (Grant No. GZSYQN[2021] 18);Guizhou Provincial Medical Research Joint Fund for High-quality Development of Health and Health Care in 2024 (Grant No. 2024GZYXKYJJXM0007); and the General Program of Guizhou Provincial Department of Science and Technology (Grant No. Qiankehe Basic MS [2025] 494).

Table 1. Comparison of predicted oral drug-likeness and pharmacokinetic profiles of the candidate compounds.

Compound	GI Absorption	Lipinski (Rule of 5)	Bioavailability Score	PAINS Alerts
Honokiol	High	Yes (0 violations)	0.55	0 alert
Rev 5901	High	Yes (0 violations)	0.55	0 alert
Caffeic acid	High	Yes (0 violations)	0.56	1 alert
Quinacrine dihy	Low	Yes (1 violation)	0.55	1 alert

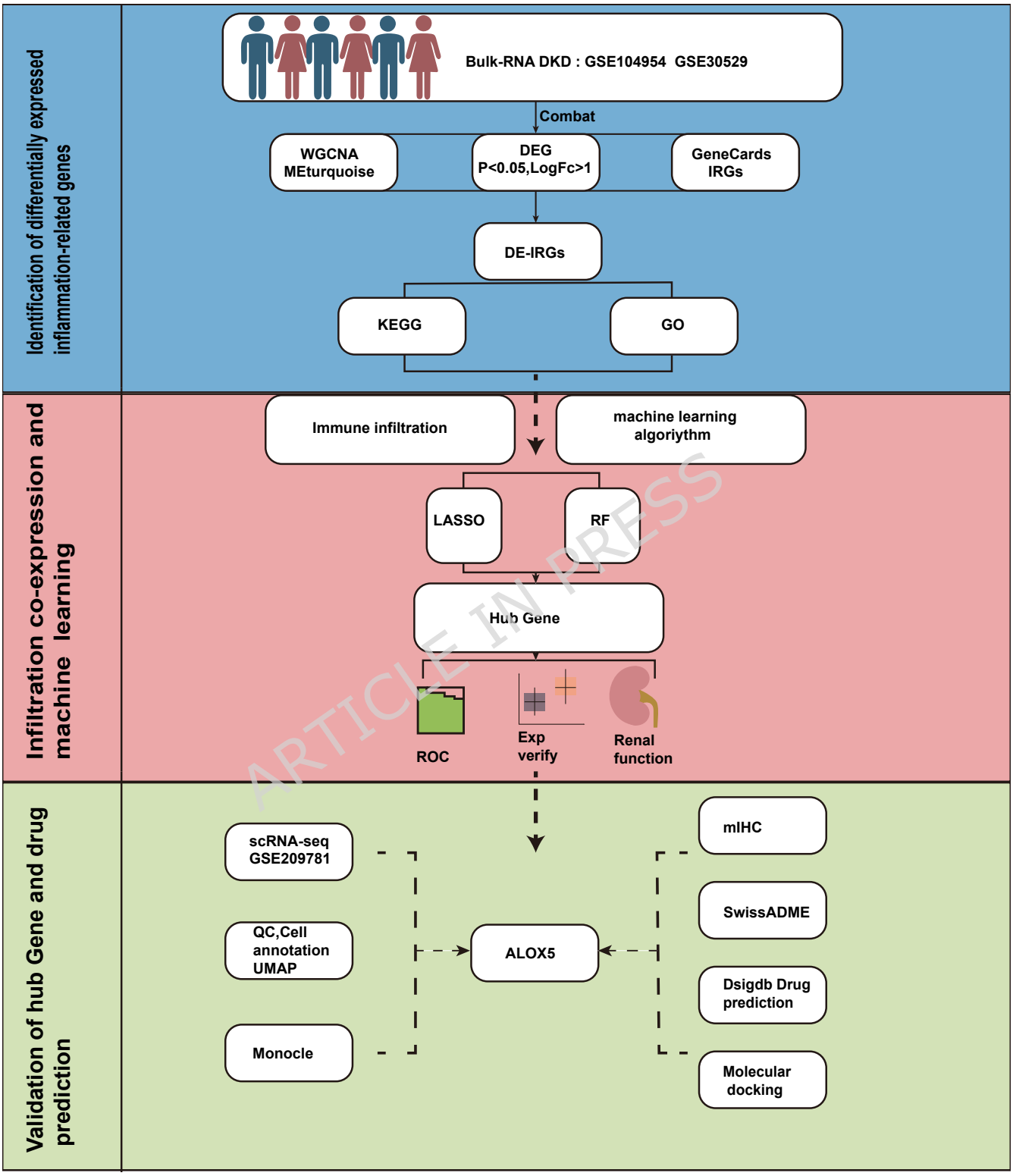

Figure 1. Study design

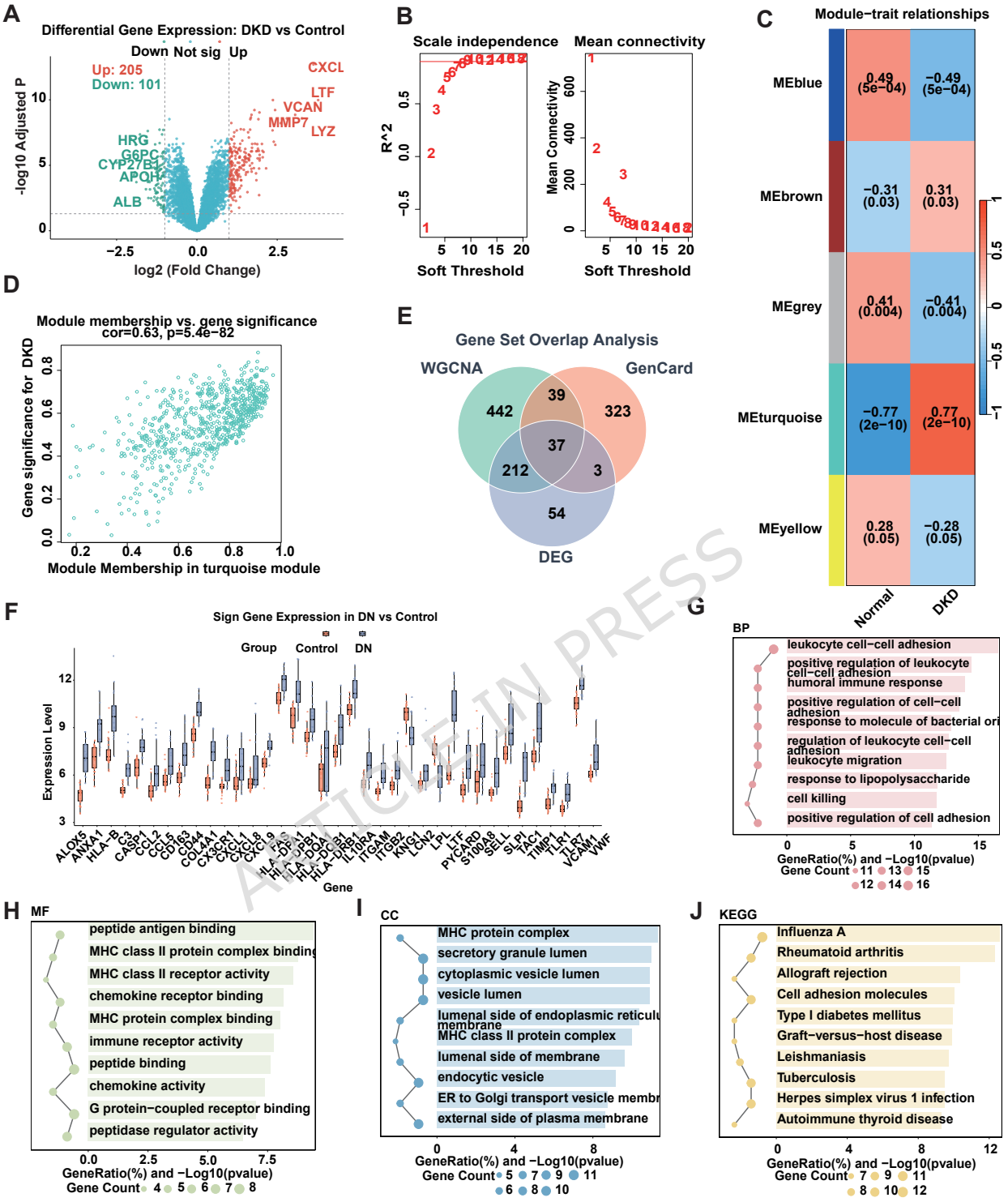

Figure 2. (A) Volcano plot displaying differentially expressed genes between DKD and control groups. (B–D) Weighted gene co-expression network analysis (WGCNA). (B) Determination of the soft-thresholding power. (C) Heatmap showing correlations between gene modules and clinical traits. (D) Scatter plot of gene significance versus module membership for the key module. (E) Venn diagram illustrating the intersection of DEGs, WGCNA module genes, and inflammation-related genes. (F) Boxplots showing the expression profiles of the 37 identified candidate genes. (G–J) Functional annotation of the candidate genes, including GO biological processes (G), molecular functions (H), cellular components (I), and KEGG pathways (J).

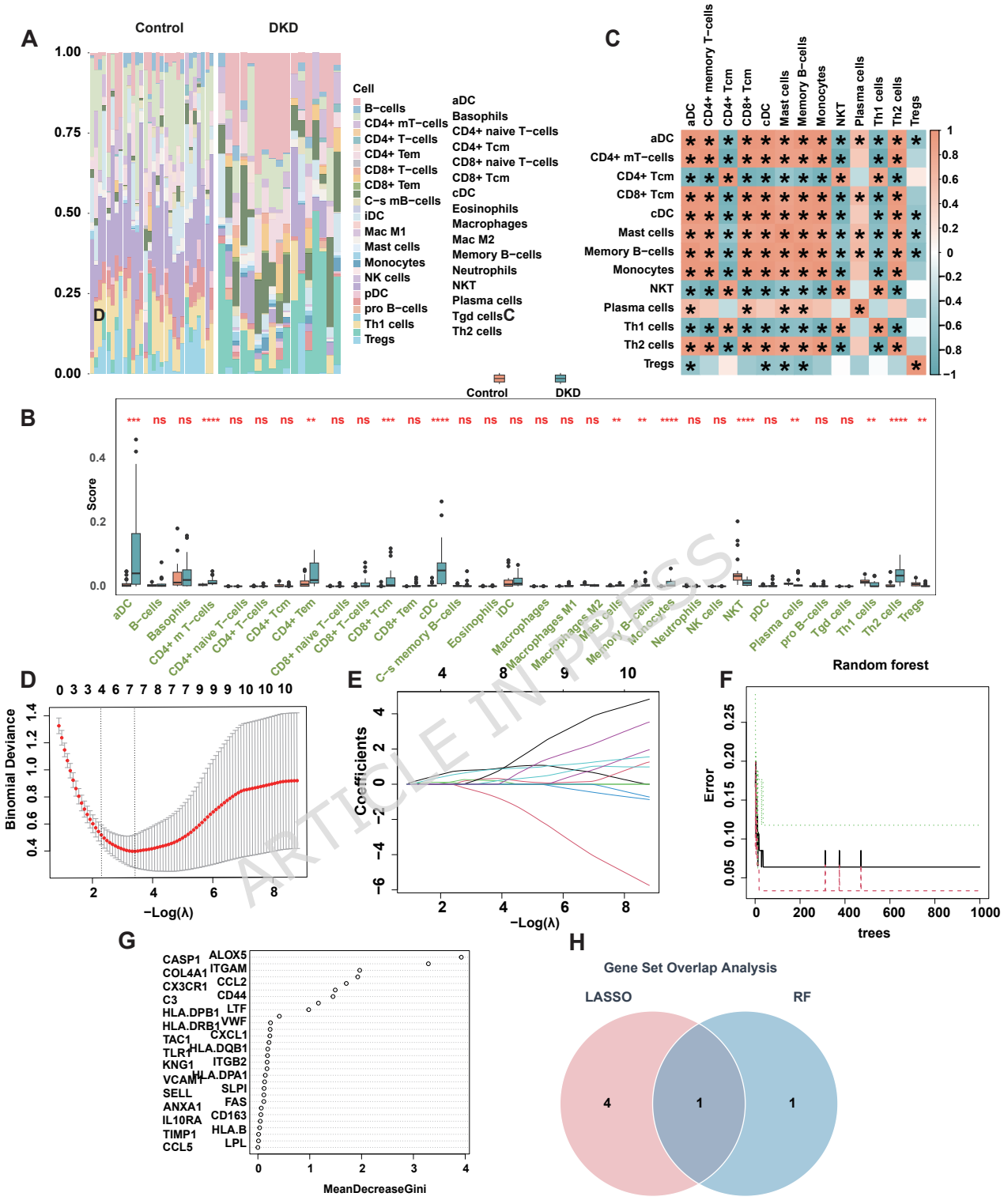

Figure 3. (A) Heatmap displaying the estimated abundance of immune cells in each sample. (B) Boxplots showing the comparison of immune cell infiltration scores between the control and DKD groups. (C) Correlation heatmap illustrating the relationships among different immune cell types. (D–E) Variable selection using the LASSO regression model, including the cross-validation plot for parameter tuning (D) and the coefficient profile plot (E). (F–G) Feature screening using the Random Forest algorithm, displaying the error rate versus the number of trees (F) and the gene importance ranking based on the MeanDecreaseGini index (G). (H) Venn diagram showing the overlap of candidate genes identified by LASSO and Random Forest analyses.

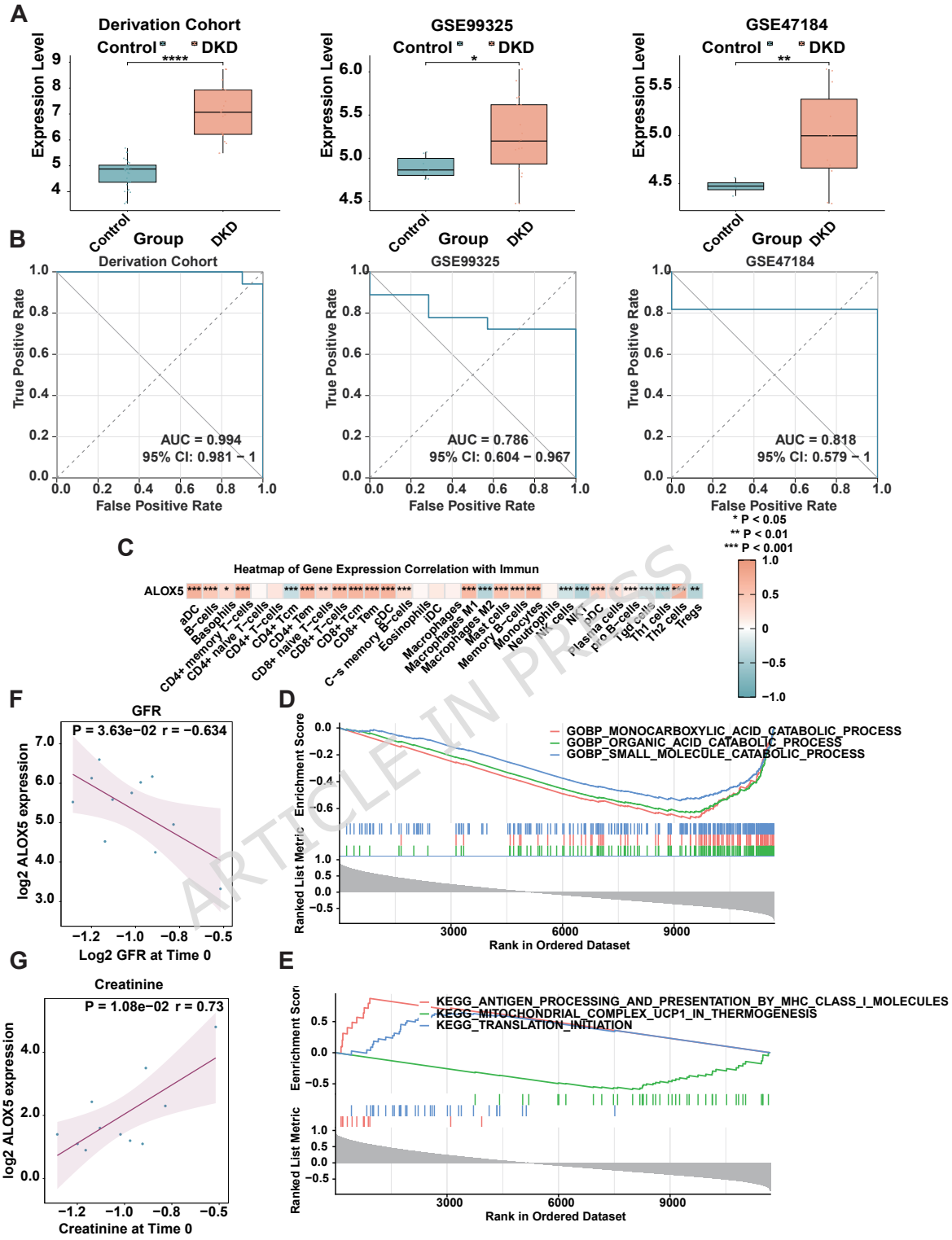

Figure 4. (A) Boxplots comparing ALOX5 expression between DKD and control samples in the derivation cohort and two external validation datasets (GSE99325, GSE47184).(B) Receiver operating characteristic (ROC) curves assessing the diagnostic accuracy of ALOX5 across the three cohorts.(C) Heatmap showing Spearman correlations between ALOX5 expression and immune cell infiltration scores.(D–E) Gene Set Enrichment Analysis (GSEA) plots identifying GO biological processes (D) and KEGG pathways (E) associated with ALOX5 expression.(F–G) Scatter plots showing the correlation of ALOX5 with glomerular filtration rate (GFR) (F) and serum creatinine (G).Data are presented as median with interquartile range in boxplots. $*P < 0.05$, $**P < 0.01$, $***P < 0.001$, $****P < 0.0001$.

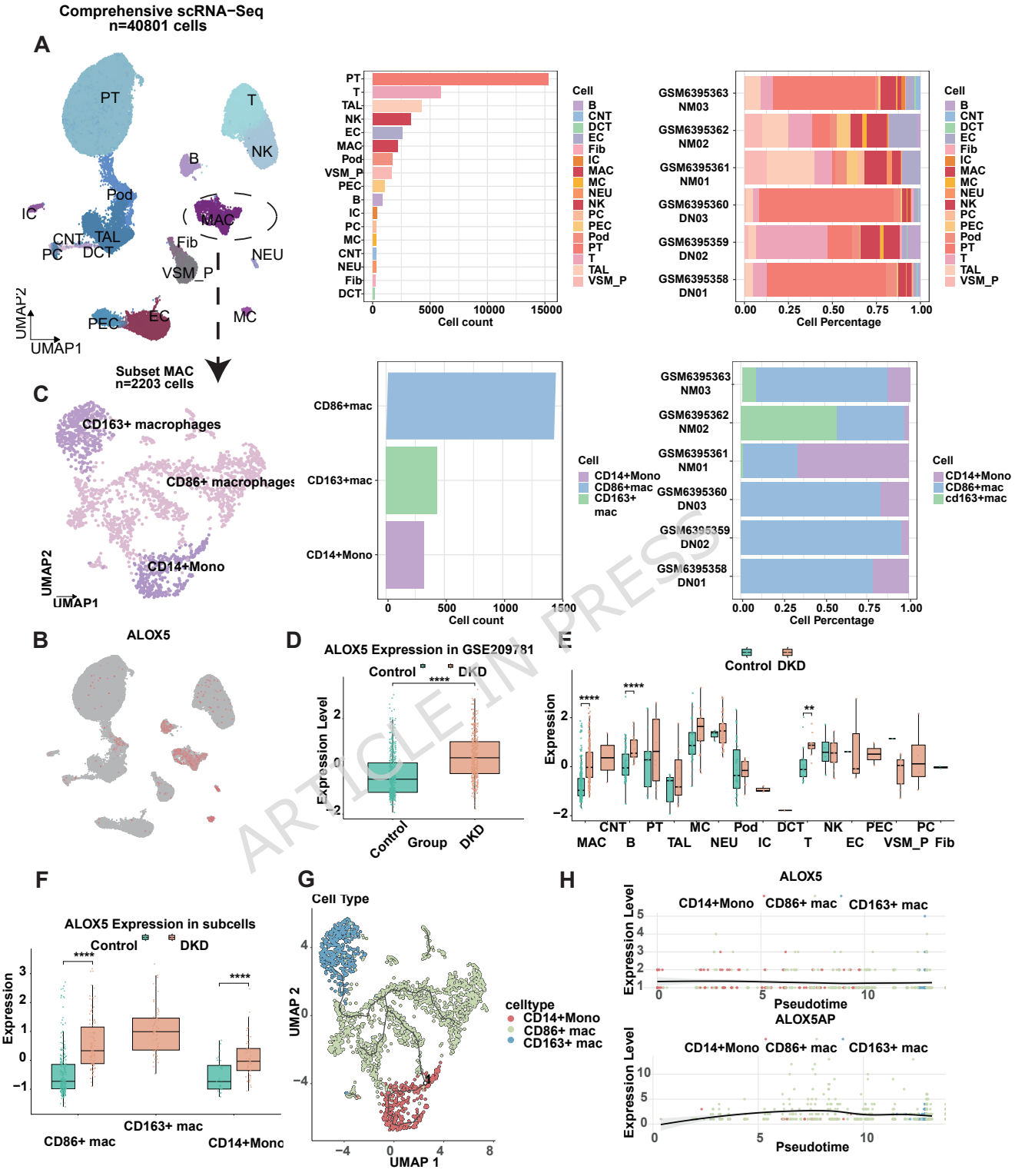

Figure 5. (A) Uniform Manifold Approximation and Projection (UMAP) visualization of 40,801 cells integrated from DKD and control samples, alongside bar plots showing cell counts and relative proportions across individuals. (B) Feature plot displaying the distribution of ALOX5 expression on the UMAP embedding. (C) UMAP plot showing the sub-clustering of the macrophage lineage into three subsets ($CD14^+$ Mono, $CD86^+$ mac, and $CD163^+$ mac), with stacked bar plots illustrating their compositional proportions. (D–F) Boxplots quantifying ALOX5 expression levels. (D) Comparison between control and DKD groups. (E) Expression across all annotated cell types split by group. (F) Expression among the three identified macrophage subpopulations.(ALOX5-positive cells after zero filtering) (G) Pseudotime trajectory analysis of macrophage differentiation constructed using Monocle3, colored by cell subtype. (H) Kinetic plots showing the expression dynamics of ALOX5 and ALOX5AP along the pseudotime trajectory. Statistical significance: $***P < 0.001$, $****P < 0.0001$.

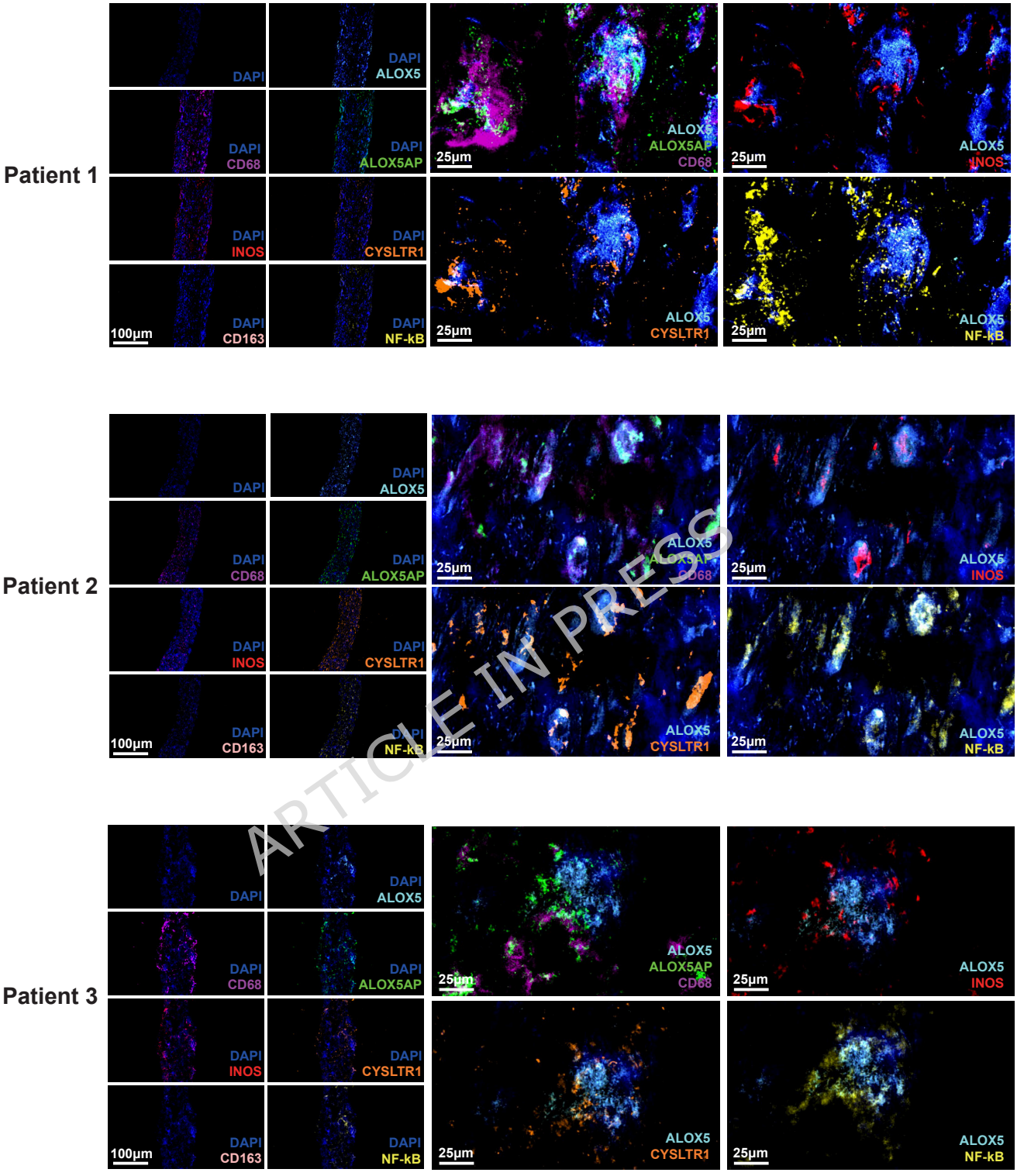

Figure 6. Multiplex immunohistochemical (mIHC) analysis of ALOX5 pathway components and macrophage phenotypes in DKD renal tissues.Representative immunofluorescence images from renal biopsies of three independent DKD patients. The panels display single-channel and merged staining for the core pathway proteins (ALOX5, ALOX5AP, CYSLTR1), the pan-macrophage marker (CD68), polarization markers (iNOS for pro-inflammatory; CD163 for anti-inflammatory), and the inflammatory transcription factor (NF-κB). High-magnification insets illustrate the spatial co-localization patterns of these proteins within the renal tubules. Nuclei were counterstained with DAPI. Scale bars: 100 μm (low magnification) and 25 μm (high magnification).The complete multichannel composite image is provided in Supplementary Fig. 4.

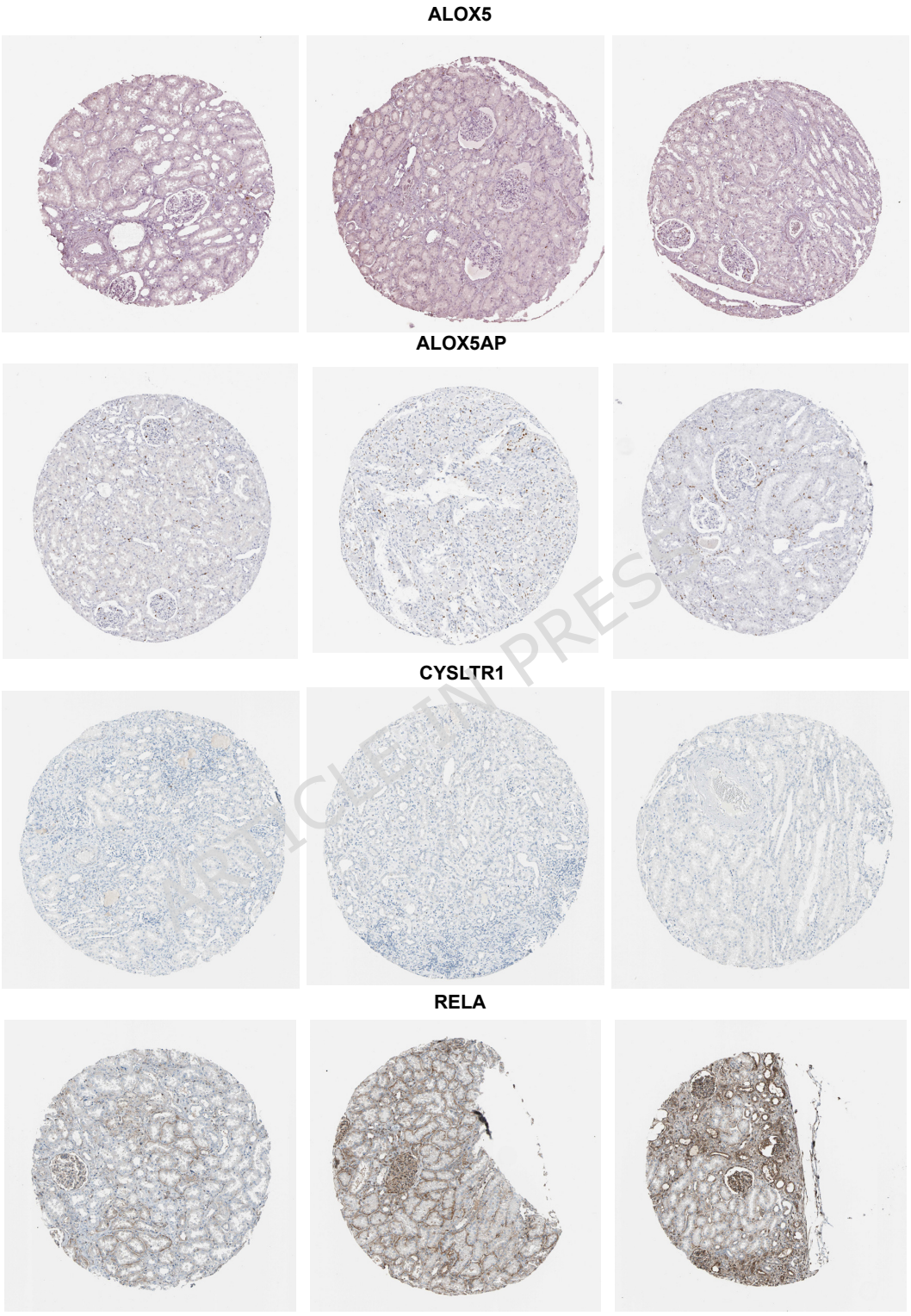

Figure 7. Representative immunohistochemistry (IHC) images retrieved from the Human Protein Atlas (HPA) database. The panels display the baseline protein expression levels of ALOX5, ALOX5AP, CYSLTR1, and RELA (NF-κB p65) in normal renal tissue microarrays.

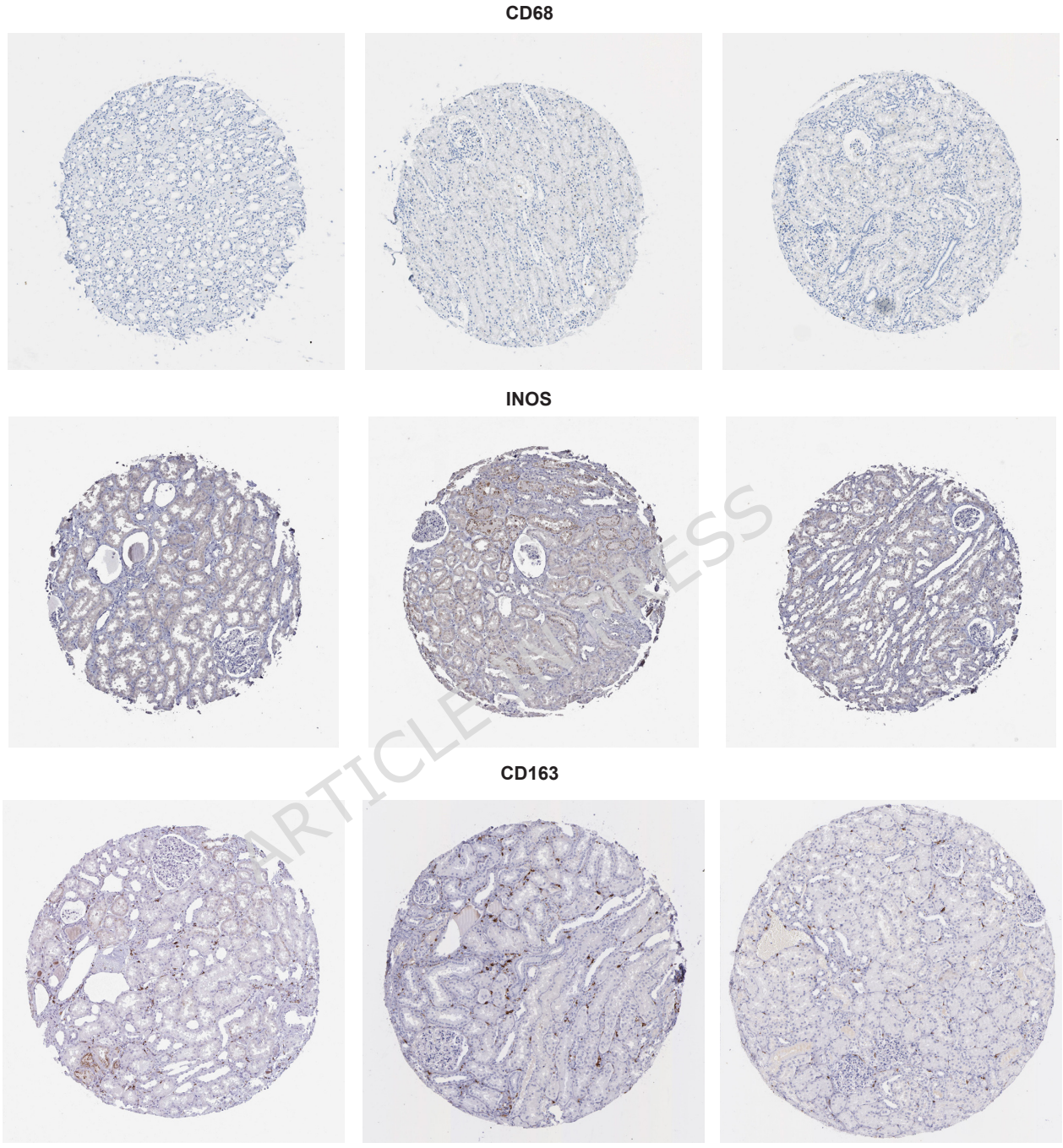

Figure 8. Representative immunohistochemistry (IHC) images retrieved from the Human Protein Atlas (HPA) database. The panels illustrate the protein expression patterns of CD68 (pan-macrophage marker), iNOS (pro-inflammatory macrophage marker), and CD163 (anti-inflammatory macrophage marker) in normal renal tissue microarrays.

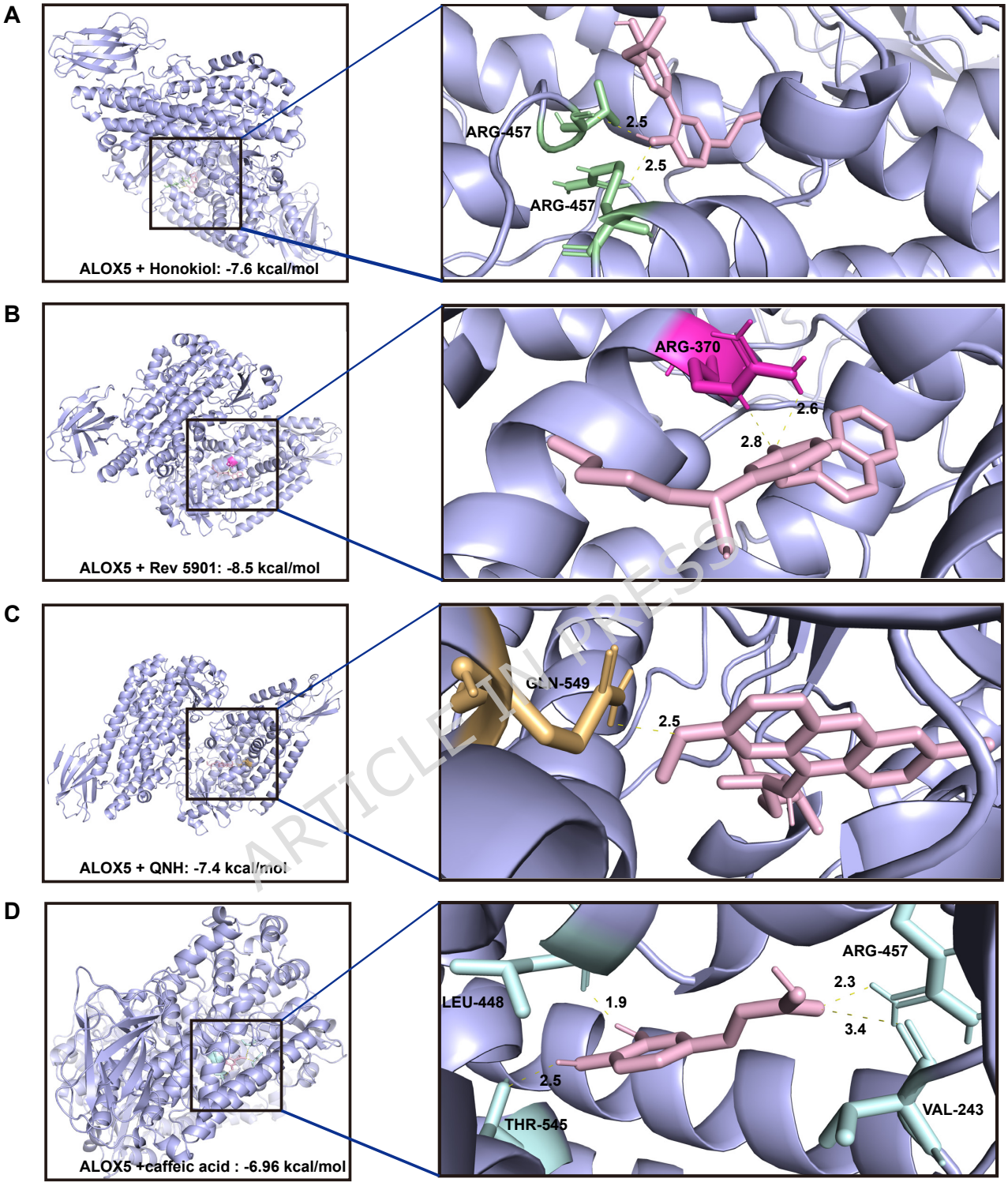

Figure 9. Visualization of the predicted binding modes between the ALOX5 protein structure and four selected compounds. For each panel, the left image displays the global view of the protein-ligand complex, while the right image provides a magnified view of the binding pocket, detailing the spatial arrangement of the ligand relative to key interacting amino acid residues. Dashed lines indicate potential interactions with corresponding distances (Å). (A) Honokiol (Binding affinity: −7.6 kcal/mol). (B) Rev 5901 (Binding affinity: −8.5 kcal/mol). (C) Quinacrine dihydrochloride (Binding affinity: −7.4 kcal/mol). (D) Caffeic acid (Binding affinity: −6.96 kcal/mol).

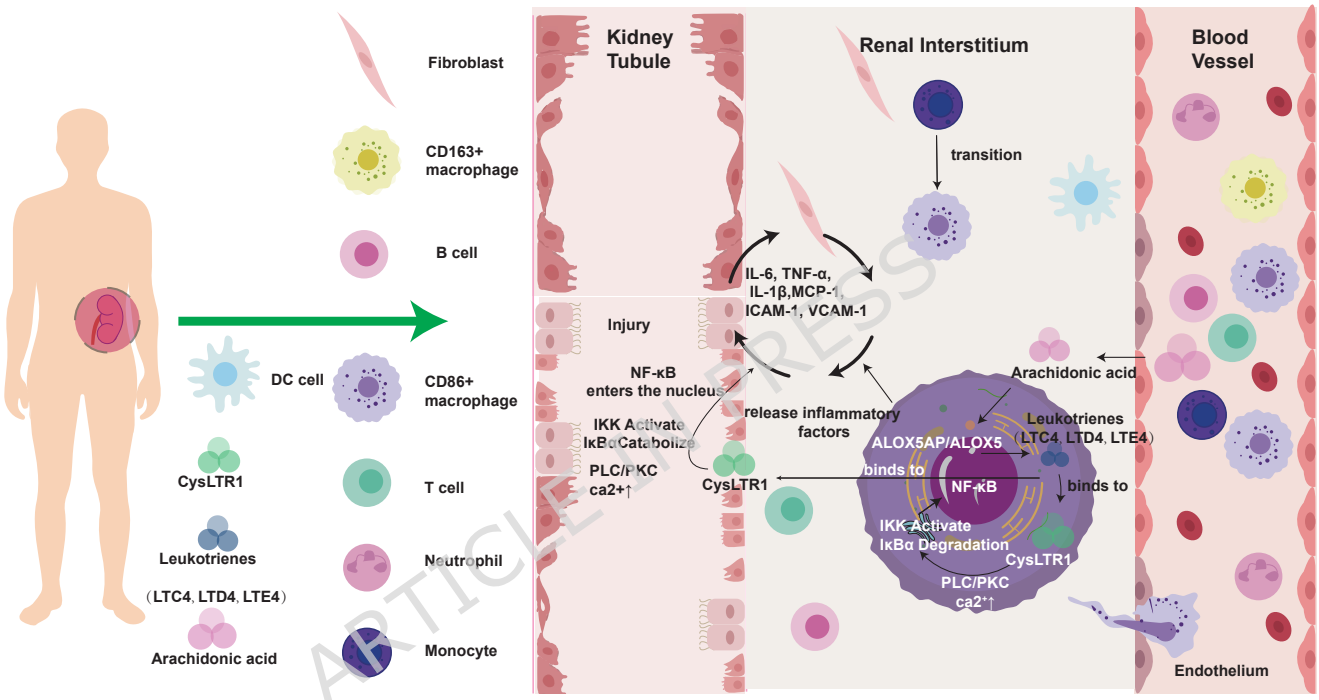

Figure 10. Proposed mechanism of the ALOX5/ALOX5AP–leukotriene–CysLTR1 axis in DKD. Infiltrating monocytes/macrophages upregulate ALOX5AP/ALOX5 to convert arachidonic acid into cysteinyl leukotrienes (LTC_4, LTD_4, LTE_4), which signal through CysLTR1 and activate PLC/PKC-mediated Ca^{2+} influx, leading to IKK activation, IκBα degradation, and NF-κB nuclear translocation. This results in increased production of pro-inflammatory mediators (IL-6, TNF-α, IL-1β, MCP-1, ICAM-1, VCAM-1) and promotes tubulointerstitial inflammation.